



# Role of Coastal Vegetation Belts in Mitigating Tsunami Waves: Bibliometric Analysis, Numerical, and Spatial Analysis

Fadly Usman<sup>1,\*</sup>, Keisuke Murakami<sup>2</sup>, Indradi Wijatmiko<sup>1</sup>, Mauhibur Rokman<sup>3</sup>, Meutia Aisyah Nabila<sup>4</sup>

<sup>1</sup>Brawijaya University, Indonesia

<sup>2</sup>University of Miyazaki, Miyazaki 889-2155, Japan

<sup>3</sup>Universitas Pesantren KH Abdul Chalim, Mojokerto, Indonesia

<sup>4</sup>Gadjah Mada University, Indonesia

\*Correspondence: E-mail: [fadlypwk@ub.ac.id](mailto:fadlypwk@ub.ac.id)

## ABSTRACT

Tsunami is a catastrophic natural disaster that is difficult to predict and often results in significant loss of life and property damage. This study examines the role of coastal vegetation belts in mitigating tsunami wave impacts through numerical and spatial analyses. This study also used bibliometric analysis to support the discussion. Numerical simulations using CADMAS Surf 2D were conducted for various scenarios to assess the effect of vegetation belts on wave speed and height. Spatial analysis using ArcGIS was employed to map tsunami-affected areas, and grid-cell analysis was used to calculate the volume of water entering inland areas during a tsunami event. The results demonstrate that vegetation belts with specific thicknesses and densities significantly reduce wave speed and height, thereby mitigating tsunami energy as it approaches land. These findings emphasize the critical role of vegetation belts in coastal management strategies. Future research should explore integrating natural barriers with artificial infrastructure, such as embankments, to provide comprehensive protection against tsunami impacts.

## ARTICLE INFO

### Article History:

Submitted/Received 25 Sept 2024

First Revised 09 Jan 2025

Accepted 22 Jan 2025

First Available online 31 Jan 2025

Publication Date 01 Mar 2025

### Keyword:

Grid cell,

Numerical simulation,

Spatial analysis,

Tsunami,

Vegetation belts.

## 1. INTRODUCTION

Indonesia is a tropical country with an extensive coastline of approximately 108,000 km, ranking it among the countries with the longest coastlines in the world. Additionally, Indonesia boasts the largest number of islands globally, with a total of 17,504 islands [1, 2]. Given this geographical reality, it is imperative to implement preventive measures and mitigation strategies to address potential disasters from the sea, such as tsunamis.

This study focuses on efforts to protect coastal areas from the risk of tsunami waves. For clarity, the term "coast" refers to the coastal hinterland extending to areas where changes in morphology, topography, and vegetation occur, whereas "beach" describes the area influenced by the ebb and flow of seawater [3].

This study involves several stages, including identifying coastal areas vulnerable to tsunami threats through spatial analysis using ArcGIS software. Additionally, numerical analysis scenarios were conducted to determine wave speed and height, with a key parameter being tsunami waves reaching 6 meters in height from the shoreline. The study also identifies areas deemed safe from tsunami waves.

Numerical simulations utilized CADMAS Surf 2D software, which applies the Navier-Stokes equation to model particle movement. This software is highly effective for disaster evaluations involving fluid materials, as it can measure various fluid behaviors, including wave height, pressure, fluid movement axis, permeability, and more.

The study's findings highlight the effectiveness of vegetation as green belts in mitigating tsunami energy and protecting coastal areas. Furthermore, the delineation of safe zones using spatial and grade-cell analysis provides practical recommendations for evacuation sites, specifically for Prigi Beach, Trenggalek, East Java, in the event of a tsunami.

## 2. METHODS

Prigi Beach is located along the southern coast of Indonesia, bordering the Indian Ocean. It is situated in Tasimadu Village, Watulimo District, Trenggalek Regency, East Java, Indonesia, approximately 48 km from the center of Trenggalek city. In addition to being a popular tourist destination, Prigi Beach serves as a national port and is home to one of the largest fishing grounds on the southern coast of Java Island. Visitors to the beach can enjoy various activities such as fishing, camping, and tennis, or simply relax at the nearby hotels while taking in the stunning coastal scenery.

As a coastal tourism destination, Prigi Beach requires robust mitigation efforts to address the threat of tsunami waves. This research involved several stages, including identifying areas at risk using spatial analysis with GIS, conducting numerical simulations with scenarios such as incorporating vegetation as green belts, comparing wave behavior with and without vegetation barriers, and identifying areas deemed safe from tsunami waves. The analysis integrated spatial and numerical simulation results with grid-cell analysis to calculate affected areas [4-6]. The grid-cell analysis method provides researchers with precise insights into disaster-affected areas by using grids of a specific size as references for preparedness and disaster prevention measures [7-11].

Spatial analysis was employed to assess the inland impact of tsunami waves, with ArcGIS software optimized to delineate affected zones and identify potential evacuation sites based on structures outside the reach of tsunami waves [12-16]. Furthermore, studies on the effectiveness of vegetation belts in reducing wave energy have produced varied results [17, 18]. Natural barrier materials such as vegetation offer a cost-effective alternative to concrete structures, such as 9-meter-high concrete walls used along Japan's Pacific coast [19].

The use of vegetation as green belts to mitigate tsunami energy entering inland areas has been explored in several previous studies, demonstrating significant reductions in wave height and speed [20-23]. Numerous researchers have also investigated the effectiveness of green belts, examining various variables such as plant height, green belt thickness, plant type, and other factors [24-28]. Equations (1)-(5) are shown in the following:

$$\frac{\partial \gamma_x u}{\partial x} + \frac{\partial \gamma_z w}{\partial z} = S_p \quad (1)$$

$$\lambda_v \frac{\partial u}{\partial t} + \frac{\partial \lambda_x u u}{\partial x} + \frac{\partial \lambda_z w u}{\partial z} = -\frac{\gamma_v}{\rho} \frac{\partial p}{\partial x} + \frac{\partial}{\partial x} \left\{ \gamma_x v_e \left( 2 \frac{\partial u}{\partial x} \right) \right\} + \frac{\partial}{\partial z} \left\{ \gamma_z v_e \left( \frac{\partial u}{\partial z} + \frac{\partial w}{\partial x} \right) \right\} - D_x u + S_u - R_x \quad (2)$$

$$\frac{\partial w}{\partial t} + \frac{\partial \lambda_x u w}{\partial x} + \frac{\partial \lambda_z w w}{\partial z} = -\frac{\gamma_v}{\rho} \frac{\partial p}{\partial z} + \frac{\partial}{\partial z} \left\{ \gamma_z v_e \left( 2 \frac{\partial w}{\partial z} \right) \right\} + \frac{\partial}{\partial x} \left\{ \gamma_x v_e \left( \frac{\partial w}{\partial x} + \frac{\partial u}{\partial z} \right) \right\} - D_z w + S_w - R_z - \gamma_v g \quad (3)$$

$$\gamma_v \frac{\partial F}{\partial t} + \frac{\partial \gamma_x u F}{\partial x} + \frac{\partial \gamma_z w F}{\partial z} = S_F \quad (4)$$

$$U = \frac{C\zeta}{H} = \zeta \sqrt{\frac{g(H+h)}{2H(H-\eta\zeta)}} \quad (5)$$

In this study, numerical analysis was conducted using CADMAS Surf 2D software, incorporating various parameters such as wave height, wave speed, fluid density, porosity, and others. The Navier-Stokes equation was utilized to simulate fluid behavior, where the x-axis and y-axis represent the positions of each fluid particle. Before the numerical simulation, the water height along the z-axis was determined. In the simulation, the function  $F(x,z,t)$  represents the ratio of water volume for each cell, where  $t$  denotes time,  $x$  the horizontal axis, and  $z$  the vertical axis in the coordinate cell [29-31].

In the Navier-Stokes equations,  $p$  represents pressure, while  $u$  and  $w$  denote the horizontal and vertical velocity components of the fluid, respectively (Agus Dwi Wicaksono & Fadly Usman, 2020; Usman & Effendi Rahim, 2017). Other parameters include  $\rho$  (rho) for fluid density,  $\nu$  for the sum of molecular kinematic viscosity and kinematic eddy viscosity,  $\gamma$  for porosity,  $\gamma_x$  and  $\gamma_z$  for the components of air porosity, and  $S_x$ ,  $S_u$ , and  $S_w$  for the sources of wave generation. The coefficients  $D_x$  and  $D_z$  represent the sponge layer, while  $R_x$  and  $R_z$  account for resistance due to porosity. Finally,  $g$  represents the acceleration due to gravity [32-34].

In Equation (5),  $U$  stands for the average depth-of-water velocity, and  $g$  denotes the acceleration due to gravity. The expression  $H = h + \zeta$  represents the total depth relative to the datum, where  $\zeta$  corresponds to the temporal bore height. Additionally,  $\eta$  is a coefficient obtained from the ratio between the initial water depth and the total propagation depth, defined as 1.03 in this research. The propagation and speed of the drill wave in this study were set following prior experimental research [35-37]. **Figure 1** illustrates a flume used in numerical simulations conducted with CADMAS Surf 2D, incorporating three measurement points. These points were used to measure wave height and wave speed at three specific locations along the X-axis: 225 m, 300 m, and 450 m. This study employs two

simulation scenarios: one without obstacles and another with natural barriers, including vegetation and topographic engineering, such as mounds of soil surrounding the green belts. Through numerical simulations using CADMAS Surf 2D, the study examines the phenomena occurring as waves pass through various barriers, including beach dunes, vegetation, elevation differences, and other obstacles, before ultimately reaching the shore.

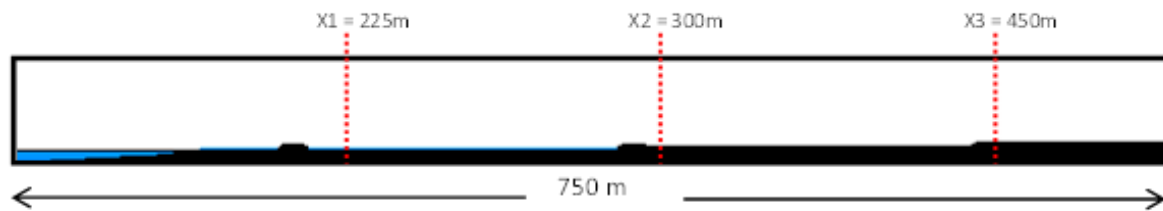


**Figure 1.** Channel (flume) used for numerical simulation by CADMAS Surf 2D.

### 3. RESULTS AND DISCUSSION

Before adding results, bibliometric analysis using the Scopus database using the keyword “tsunami” taken on January 2025 (see **Figure 2**). The figure illustrates the number of documents published per year, combining a table and a line curve to provide an overview of publication trends. The table on the left highlights the annual number of documents from 2016 to 2024, showing fluctuations over the years. The highest publication count is observed in 2022 with 1,729 documents, followed by a gradual decline in subsequent years. The line curve on the right provides a longer-term view, spanning from 1929 to 2024. It reveals minimal publication activity until the late 1990s, after which there was a significant and rapid increase. The number of documents peaks in the early 2010s, followed by slight fluctuations and a gradual decline in recent years. This trend likely reflects advancements in digital technology and increased research activities over the decades. However, the slight reduction in recent years may indicate a shift in research focus or external factors affecting research productivity.

Given the increasing frequency and devastating impacts of tsunamis, particularly in coastal regions worldwide, there is a pressing need for continued and intensified research in this field. Tsunami research plays a crucial role in developing effective mitigation strategies, enhancing early warning systems, and improving coastal resilience. The decline in recent publication trends underscores the importance of sustaining and expanding research efforts to address the challenges posed by tsunamis and to safeguard vulnerable communities.

The study conducted simulations using two scenarios: (1) without obstacles and (2) with natural obstacles, including vegetation and limited topographic engineering in the form of mounds and excavations. The following images present screenshots of the simulation for scenario #1. **Figure 3** illustrates the propagation of waves as they travel from the foreshore and move inland.

Initially, tsunami wave barriers occur on the foreshore, but the wave propagates inland with relative ease in this scenario due to the absence of significant obstacles to reduce the horizontal force of the wave. Although minor obstacles, such as surface irregularities and topographic variations in the coastal area, are present in scenario #1 of the numerical simulation, these features are not substantial enough to significantly reduce wave speed or mitigate the tsunami energy entering the land.

The wave phenomenon in scenario #1 is depicted in the profile shown in **Figure 4**. The orange line represents the wave height at measurement point  $x_3=450$  m. At this location, the

wave height remains considerable, measuring approximately 2.5–3.0 m. Initially, the wave height from the simulation ranged between 5.75 and 6.25 m, with a reduction of around 2.38 m. The limited surface resistance allows the wave to propagate further inland. This indicates that the waves reaching the land consist primarily of runoff residuals traveling from the beach to the inland areas.

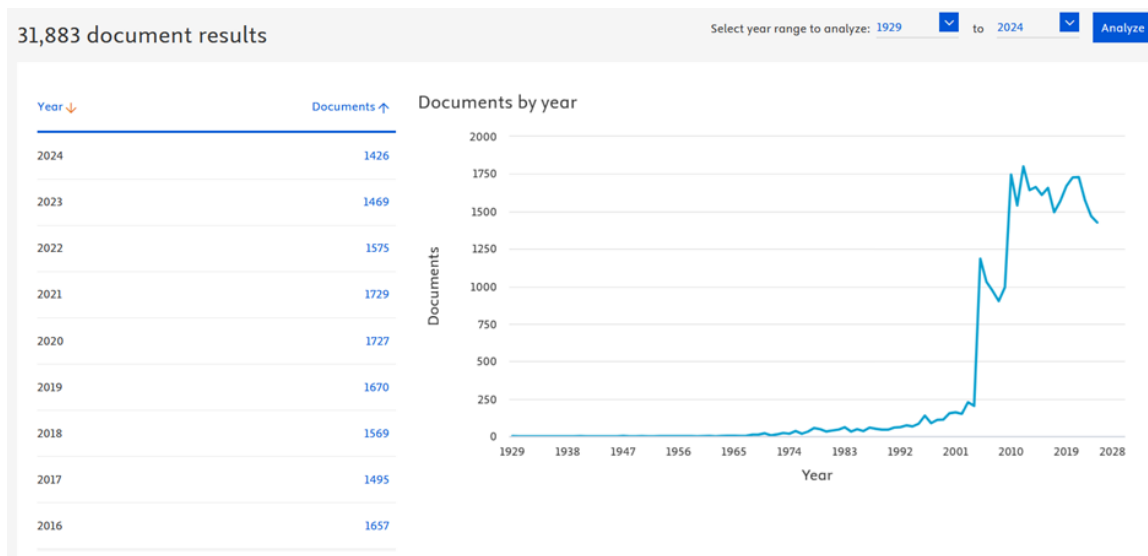


Figure 2. Publication trend in Scopus regarding tsunamis.



Figure 3. Snapshot of tsunami propagation in scenario #1.

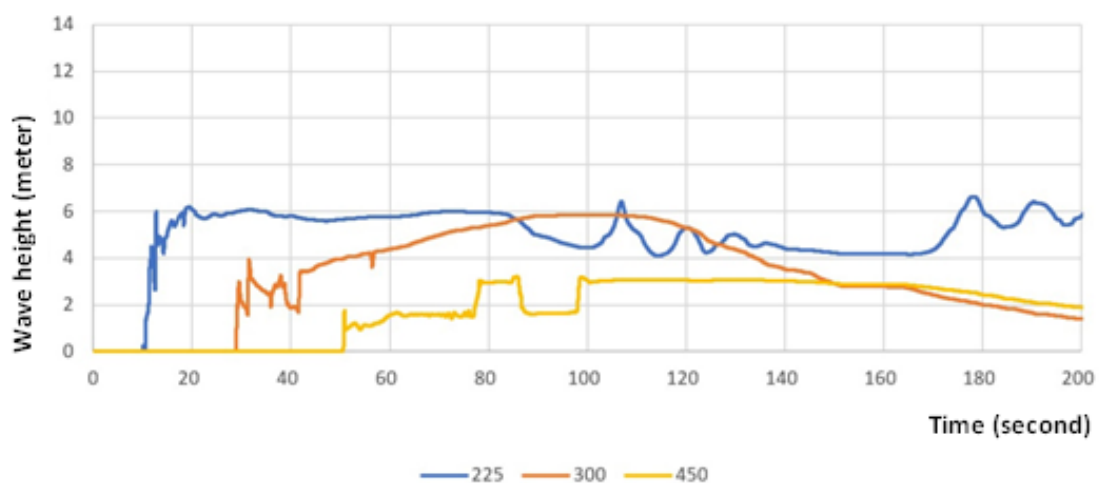


Figure 4. Wave height in scenario #1.

Although the wave height in this simulation is set using the Fukui equation, ranging from 6.0 to 10.0 m, the sea waves with bore wave formation break upon reaching the foreshore (see **Table 1**). The wave heights gradually decrease from the initial range of 6 to 10 m at the start of the simulation to less than 5 m by the measurement point at 450 m. Beyond this point, the wave continues to propagate inland, with heights ranging from approximately 2.78 to 3.79 m.

**Table 1.** Wave speed and wave height in the simulation.

Wave Height	Water level (m)			Wave speed (m/s)		
	X1	X2	X3	X1	X2	X3
6 m	5.45	3.17	2.38	6.05	5.05	3.21
8 m	7.14	4.58	2.78	6.35	5.11	3.36
10 m	8.84	6.38	3.79	6.38	5.25	3.67

**Figure 5** illustrates wave propagation in scenario #2. Initially, the tsunami wave encounters barriers on the foreshore, followed by additional obstacles in the conservation zone. The wave volume is further blocked due to elevation differences and the site plan of the generator unit. Vegetation in the conservation zone serves as a horizontal force reducer, slowing the water before it advances inland.

The profile in **Figure 6**, represented by the orange line, shows the wave height at measurement point x3=450 m. At this location, the wave height remains relatively high, approximately 2.5–3.0 m. Initially, the wave height in the simulation ranges from 5.75 to 6.25 m, with a reduction of about 2.25 m. The surface resistance ultimately allows a portion of the wave to reach inland. This indicates that the waves reaching the land consist primarily of runoff residuals traveling from the beach to the inland areas.

As shown in **Figure 5**, the screenshot depicts the results of the numerical simulation for the second scenario. Wave propagation from the shoreline advances inland after encountering several obstacles. Initially, the tsunami waves are blocked at the shoreline and sand dunes (beach area). The next obstacle occurs as the waves overtop the embankment between the coastal area and the shore, filling the conservation zone with trapped water.

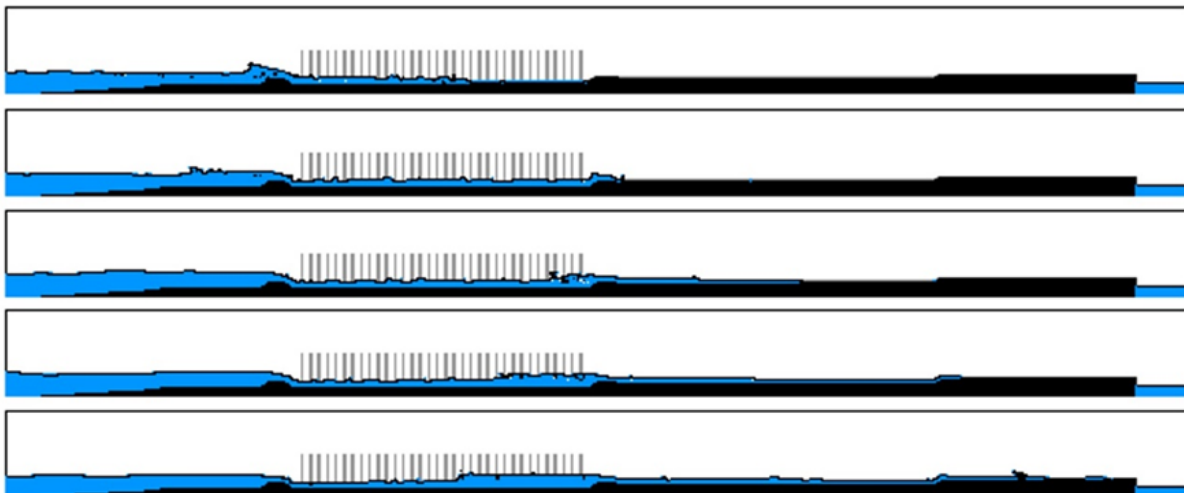


**Figure 5.** Snapshot of tsunami propagation in scenario #2.

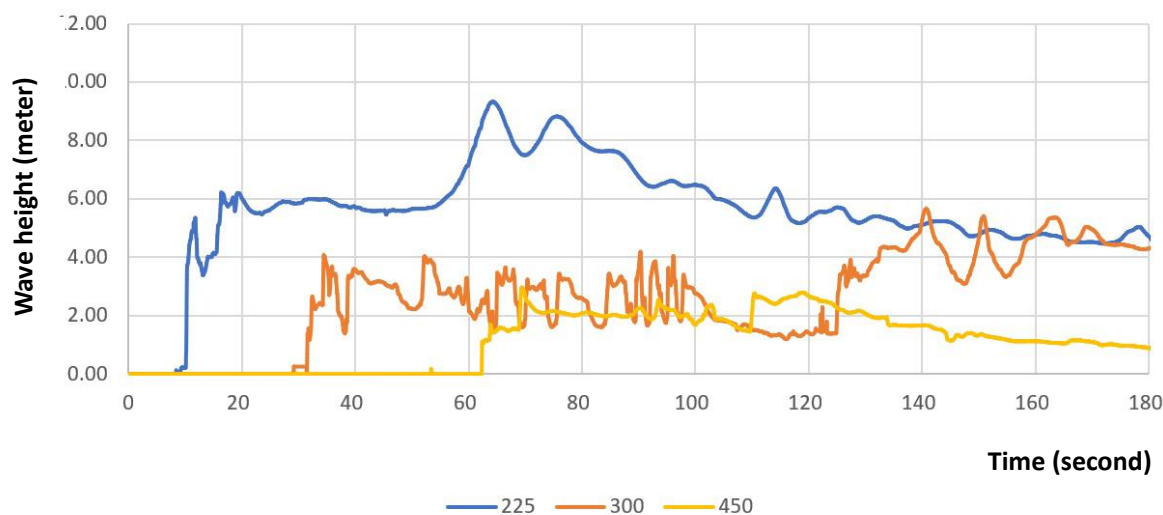


**Figure 6.** Wave height in scenario #2.

The phenomenon observed in the conservation area indicates that the tsunami wave is initially dampened by precast constructions and beach fencing. Additionally, due to elevation differences, turbulence arises around the embankment. The waves then propagate through the green belt and continue inland, eventually reaching the edge of the generator site. The wave volume is temporarily held in the precast formation pool and beachside constructions before advancing into the conservation area, where the vegetation belts contribute to further reducing the wave energy.

**Figure 6** presents the wave height results from the simulation in scenario #2. At the shoreline, near the 225 m measurement point, the wave exhibits a rapidly fluctuating profile. However, by the 300 m measurement point, the accumulated wave height begins to stabilize compared to the more erratic behavior observed at 225 m. At the 450 m measurement point, approximately 400 m inland, the wave height rises dramatically but remains below 1 m.

At  $x=450$  m, wave speed measurements indicate minimal activity, suggesting that only secondary waves manage to propagate inland after being trapped in the conservation zone. This finding highlights the effectiveness of the green belt in reducing wave speed and demonstrates how the embankment constructed within the conservation zone serves as a significant obstacle to tsunami propagation.

**Figure 7** provides further insights, with the orange line representing the wave height at  $x=450$  m, following its interaction with the conservation zone. The wave height within the conservation zone and vegetation belts remains significant, as shown by the blue line profile in **Figure 7**. The profile remains relatively level until about 100 m, after which fluctuations in wave height are observed, indicating the wave's residual energy. This suggests that the waves reaching inland are runoff residuals from the conservation zone, further dampened by the vegetation belts.

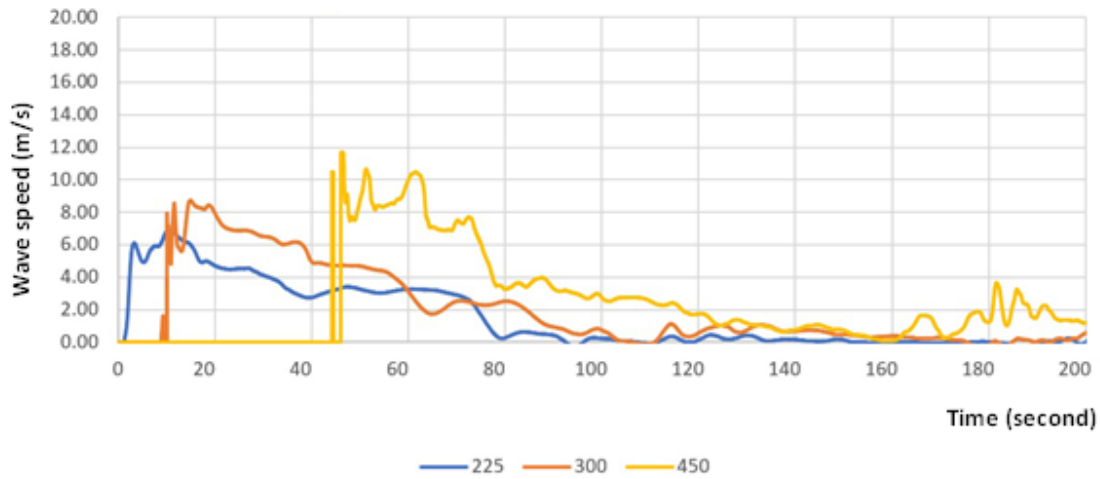


**Figure 7.** Wave speed in scenario #2.

**Figure 7** shows the results of wave speed measurements based on the simulation in scenario #3. At the measurement point X1=225 m, the wave initially arrives at a normal speed, ranging from approximately 6.0 to 7.0 m/s. However, by the 300 m measurement point, turbulence caused by shoreline obstacles, including embankment constructions and green belts, significantly reduces the average wave velocity to about 4.0 to 5.5 m/s. At the 450 m measurement point, the wave speed drops even further, reaching a range of approximately 1.25 to 2.5 m/s as it continues inland. **Table 2** presents the measurements of wave height and wave speed for different initial wave heights (6, 8, and 10 m). The decrease in wave energy begins at the X1 measurement point but becomes more pronounced as the wave accumulates in the pond at the X2 measurement point. By the time the wave reaches the power plant zone, its height is reduced to approximately 1 m, with a velocity of around 1.25 m/s. This significant reduction demonstrates the effectiveness of the implemented obstacles in mitigating the overall tsunami energy.

**Table 2.** Wave speed and wave height in the simulation.

Wave Height	Water level (m)			Wave speed (m/s)		
	X1	X2	X3	X1	X2	X3
6 m	6.20	2.80 - 4.12	0.95	6.85	4.53	1.50
8 m	6.81	5.35 - 6.05	1.35	6.98	5.06	1.83
10 m	8.95	6.15 - 9.27	1.89	7.11	5.13	2.15

**Figure 8** illustrates the delineation of the affected area, created using spatial analysis by processing elevation model (DEM) data with a topographic height limit of up to 20 m. This maximum assumption is based on findings from previous research, which indicate that tsunami waves can travel inland up to approximately 3.5 km from the shoreline and reach heights of about 20 m above sea level. The propagation of waves accumulating in the coastal area continues inland due to the significant volume of seawater entering the land. This explains why tsunami waves can travel considerable distances from the shoreline [38, 39].

**Figure 9** depicts a grid-cell overlay applied to a tsunami-affected map to estimate the volume of water entering the land. The grid-cell analysis results, based on the numerical simulation in scenario #2 (featuring vegetation belts and topographic engineering), are displayed on the map. Each grid measures 50 x 50 m<sup>2</sup>, and the vegetation belts serving as the conservation zone range from 100 to 250 m in width from the shoreline. Vegetation belts and

topographic arrangements significantly reduce tsunami energy, wave speed, and wave volume. While the vegetation belt thickness in simulation #2 is set at approximately 100 m, **Figure 9** depicts belt thicknesses of 100–250 m, adapted to the availability of coastal land and following a similar planting pattern as in scenario #2, with a planting distance of 5 m.

Vegetation belts or conservation areas, such as mangrove forests, coastal forests, or other plants, can mitigate the impact of tsunamis. Their effectiveness depends on several factors, particularly their ability to reduce wave energy. Vegetation belts absorb some tsunami energy through friction between water and the trees, roots, and soil surface. Dense and robust vegetation can slow water flow, reducing tsunami wave speed and intensity. Vegetation belts also reduce wave currents by decelerating water, diminishing the destructive force of tsunamis when they reach settlements or critical assets. Additionally, tree roots, like those of mangroves, prevent soil erosion caused by tsunamis. Vegetation belts contribute to wave dispersion by breaking up water waves, causing the water to spread and reducing its destructive power in areas behind the vegetation [40-42].

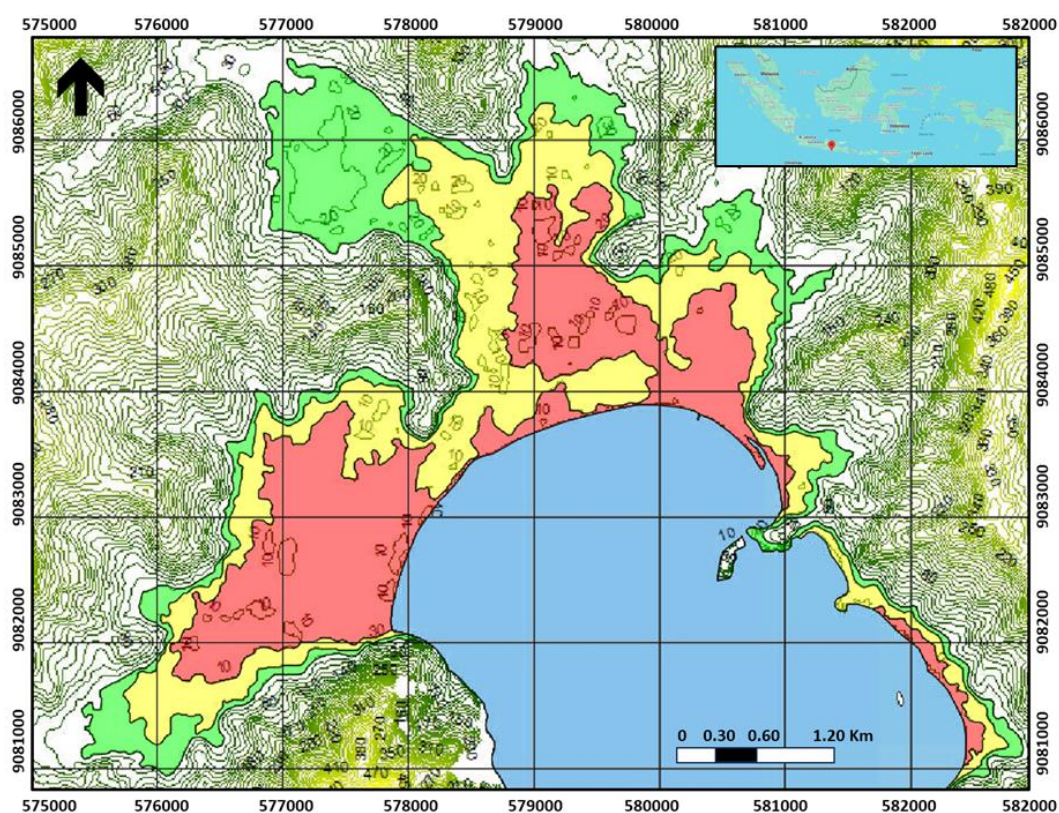


**Figure 8.** Areas at risk of tsunami impact through elevation data analysis.

In **Figure 9**, the yellow dotted line represents the predicted tsunami wave boundary after being dampened by vegetation belts 100–250 m thick from the shoreline. This prediction is derived from the numerical simulation results in scenario #2, where vegetation belts effectively reduce tsunami wave speed and volume. However, vegetation belts have limitations in mitigating wave height. If incoming tsunami waves are 8 or 10 m high and the vegetation is only 2 or 3 m tall, the waves can easily surpass the vegetation. The type and density of vegetation also play a critical role. Trees with strong, spreading roots, such as mangroves, are most effective, as they anchor the soil well. In contrast, sparse vegetation or fragile plants like shrubs or crops (e.g., rice, corn, or sugarcane) provide minimal resistance. Furthermore, even if the vegetation belt is 100 m thick, inadequate tree density or weak

vegetation types may allow large tsunami waves to pass through, resulting in significant damage.

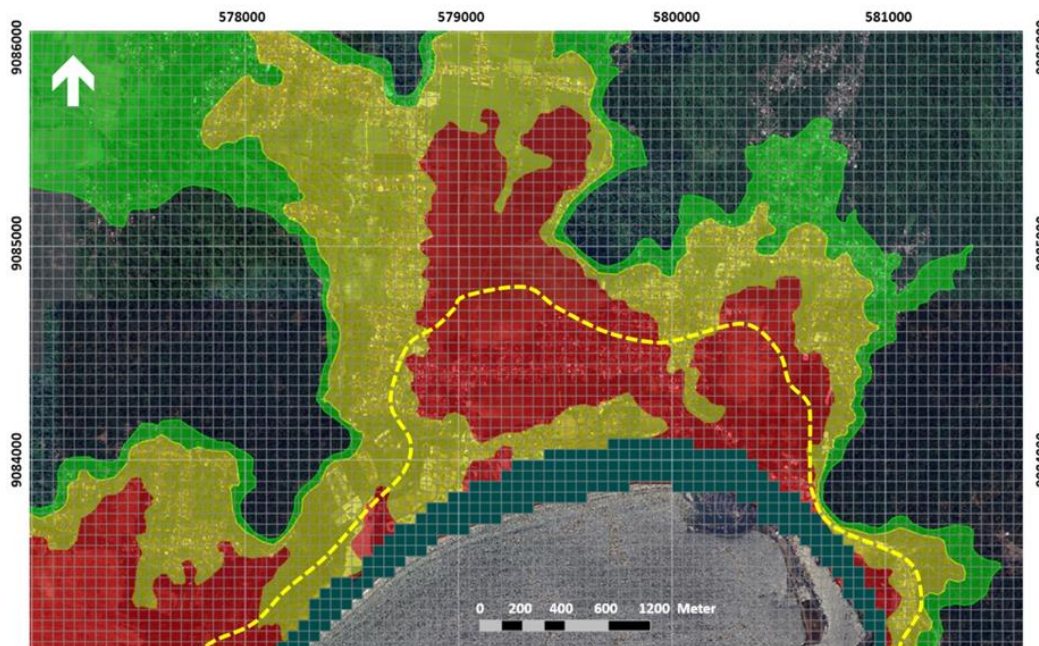


**Figure 9.** Vegetation belts on coastal area to reduce tsunami energy by grid-cell analysis.

#### 4. CONCLUSION

Based on the analysis results, several recommendations can be proposed for the Prigi Beach coastal area. Vegetation belts or conservation zones are effective in reducing the impact of tsunami waves due to their ability to act as barriers. This is enhanced by the presence of a green belt within the conservation zone and elevation differences between the conservation zone and the coastal area of Prigi Beach. The mounds between the conservation zone and the coastal area effectively inhibit wave propagation, trapping the waves in the vegetation belts or conservation zones.

At the 450 m measurement point, located in the residential and agricultural areas, only limited runoff from the conservation zone is observed. However, preventive measures are still necessary, such as constructing mounds or ditches around the vegetation zone with sufficient height and depth. While the seawater is largely trapped within the vegetation belts or conservation zones, additional measures are needed to protect critical assets, such as houses and agricultural fields. To further mitigate the propagation of primary waves, additional traps, such as ditches or drainage channels, should be strategically placed around village assets, integrated with appropriate topographic arrangements and landscape designs for the coastal area of Prigi Beach.

Vegetation belts can significantly reduce tsunami impacts when they are well-designed, utilizing appropriate plant species and integrating topographic engineering, as demonstrated in scenario #2 of the numerical simulation. The thickness and density of the vegetation are crucial for absorbing tsunami energy. However, vegetation belts with limited heights (e.g., 2–3 m) may not be sufficient to withstand large tsunami waves with heights of 6–10 m. Despite this, waves propagating inland typically decrease in height, emphasizing the importance of maintaining robust vegetation belts.

Future research should explore the potential of combining vegetation belts with artificial infrastructure, such as embankments or breakwaters. This integrated approach could provide

more effective protection by further dampening tsunami energy, reducing wave speed, and minimizing the height of tsunami waves that reach coastal and residential areas.

## 5. ACKNOWLEDGMENT

The author expresses gratitude to Faculty of Engineering, and the Research and Community Service of Brawijaya University, Indonesia for providing funding for this research. Special acknowledgment is given to Professor Keisuke Murakami from Miyazaki University, who contributed to the research through research collaborative program between Brawijaya University, Indonesia and University of Miyazaki, Japan.

## 6. REFERENCES

- [1] Mattiro, S., Widaty, C., and Apriati, Y. (2023). Historical cultural maritime notes and the integration of its values in shaping the self-reliance of coastal Ecotourism. *Yupa: Historical Studies Journal*, 7(2), 194-210.
- [2] Heo, S., Sohn, W., Park, S., and Lee, D. K. (2024). Multi-hazard assessment for flood and Landslide risk in Kalimantan and Sumatra: Implications for Nusantara, Indonesia's new capital. *Heliyon*, 10(18), e37789.
- [3] Short, A. D., and Short, A. D. (2020). The Australian coast: Introduction. *Australian Coastal Systems: Beaches, Barriers and Sediment Compartments*, 32, 1-81.
- [4] He, W., Li, X., Zhou, Y., Liu, X., Gong, P., Hu, T., Yin, P., Huang, J., Yang, J., Miao, S., Wang, X., and Wu, T. (2023). Modeling gridded urban fractional change using the temporal context information in the urban cellular automata model. *Cities*, 133, 104146.
- [5] Usman, F., Chalim, S., Usman, F., Fathoni, M., Rozikin, M., Saputra, H., and Murakami, K. (2024). Assessing coastal population capacity in Tsunami-prone areas: A grid-based approach. *Jàmbá Journal of Disaster Risk Studies*, 16(1), 1–11.
- [6] Wang, Y., Zhang, C., Chen, A. S., Wang, G., and Fu, G. (2023). Exploring the relationship between urban flood risk and resilience at a high-resolution grid cell scale. *Science of The Total Environment*, 893, 164852.
- [7] Ajtai, I., Ștefănie, H., Maloș, C., Botezan, C., Radovici, A., Bizău-Cârstea, M., and Baciuc, C. (2023). Mapping social vulnerability to floods. A comprehensive framework using a vulnerability index approach and PCA analysis. *Ecological Indicators*, 154, 110838.
- [8] Guelleh, H. O., Patel, R., Kara-Zaitri, C., and Mujtaba, I. M. (2023). Grid connected hybrid renewable energy systems for urban households in Djibouti: An economic evaluation. *South African Journal of Chemical Engineering*, 43, 215–231.
- [9] Li, C., and Bacete, G. (2022). Mapping the technology footprint in design for social innovation. *International Journal of Innovation Studies*, 6(3), 216–227.
- [10] Roy, S., Majumder, S., Bose, A., & Chowdhury, I. R. (2024). Mapping the vulnerable: A framework for analyzing urban social vulnerability and its societal impact. *Societal Impacts*, 3, 100049.
- [11] Wang, W., Kim, D., Han, H., Tak Kim, K., Kim, S., and Soo Kim, H. (2023). Flood risk assessment using an indicator-based approach combined with flood risk maps and grid data. *Journal of Hydrology*, 627, 130396.

- [12] Fefta, A., Usman, F., Wicaksono, A. D., Utomo, D. M., and Murakami, K. (2023). Public policy management in determining the feasibility of the smart city project in Malang, Indonesia. *International Journal of Sustainable Development and Planning*, 18(3), 677–682.
- [13] Nugroho, A., Hasyim, A., and Usman, F. (2018). Urban growth modelling of Malang city using artificial neural network based on multi-temporal remote sensing. *Civil and Environmental Science*, 1(2), 052–061.
- [14] Turniningtyas Ayu Rachmawati, Alnardo Bimacakra Fisabilhakh, and Usman, F. (2024). Disaster evacuation point and evacuation road plan kedunglarangan river flood at bangil sub-district Pasuruan regency. *Evergreen*, 11(2), 1167–1181.
- [15] Usman, F., Hariyani, S., Kurniawan, E. B., and Sari, I. C. (2023). Measuring resilience of a tourism village against flash flood disaster. *Regional and Rural Studies*, 1(1), 15–21.
- [16] Usman, F., Wardhani, J. K., Sari, I. C., and Chalim, S. (2023). Assessing trauma healing methods for volcanic disaster evacuees in Indonesia. *Journal Européen Des Systèmes Automatisés*, 56(6), 1019–1025.
- [17] Hari Ram, N., and Sriram, V. (2024). Energy dissipation characteristics in vegetation belt due to mono-chromatic and bi-chromatic waves. *Ocean Engineering*, 312, 119062.
- [18] Wang, Y., Wang, G., Sun, J., Song, C., Lin, S., Sun, S., Hu, Z., Wang, X., and Sun, X. (2024). The impact of extreme precipitation on water use efficiency along vertical vegetation belts in Hengduan Mountain during 2001 and 2020. *Science of The Total Environment*, 943, 173638.
- [19] Usman, F., and Effendi Rahim, S. (2017). Investigate the Effectiveness of Seawall Construction using CADMAS Surf 2D. *MATEC Web of Conferences*, 97, 01065.
- [20] Farahdita, W. L., and Siagian, H. S. R. (2020). Analysis of the area affected by the tsunami in Pandeglang, Banten: A case study of the Sunda Strait Tsunami. *IOP Conference Series: Earth and Environmental Science*, 429(1), 012052.
- [21] Hamzah, L., Puspito, N. T., And Imamura, F. (2000). Tsunami catalog and zones in Indonesia. *Journal of Natural Disaster Science*, 22(1), 25–43.
- [22] Lavigne, F., Gomez, C., Giffò, M., Wassmer, P., Hoebreck, C., Mardiatno, D., Prioyono, J., and Paris, R. (2007). Field observations of the 17 July 2006 Tsunami in Java. *Natural Hazards and Earth System Sciences*, 7(1), 177–183.
- [23] Usman, F., Wicaksono, A. D., and Setiawan, E. (2016). Evaluation of the reduction of tsunami damages based on local wisdom contermesures in Indonesia. *Review of European Studies*, 8(1), 157.
- [24] Kurosawa, T. (2021). Facility against tsunamis and green infrastructure—a case study of post-disaster reconstruction after the Great East Japan Earthquake. *Coastal Engineering Journal*, 63(3), 200–215.
- [25] Pertiwi, I. I., Fattah, M. H., and Rauf, A. (2018). Estimation of tsunami inundation and disaster mitigation in Bulukumba, Indonesia. *Jurnal Geofisika*, 16(1), 1.
- [26] Strusińska-Correia, A. (2017). Tsunami mitigation in Japan after the 2011 Tōhoku Tsunami. *International Journal of Disaster Risk Reduction*, 22, 397–411.

- [27] Suppasri, A., Al'ala, M., Luthfi, M., and Comfort, L. K. (2019). Assessing the tsunami mitigation effectiveness of the planned Banda Aceh Outer Ring Road (BORR), Indonesia. *Natural Hazards and Earth System Sciences*, 19(1), 299–312.
- [28] Zaitunah, A., Samsuri, and Slamet, B. (2018). Analysis of gin Sibolga for tsunami Mitigation. *IOP Conference Series: Earth and Environmental Science*, 166, 012028.
- [29] Khechekhouche, A., Benhaoua, B., Driss, Z., Attia, M. E. H., and Manokar, M. (2020 A). polluted groundwater treatment in southeastern Algeria by solar distillation. *Algerian Journal of Environmental and Sciences*, 6(1).1207-1211.
- [30] Suharyanto, A. (2012). Predicting tsunami inundated area and evacuation road based on local condition using GIS. *IOSR Journal of Environmental Science, Toxicology and Food Technology*, 1(4), 05–11.
- [31] Watts, P. (1998). Wavemaker curves for tsunamis generated by underwater landslides. *Journal of Waterway, Port, Coastal, and Ocean Engineering*, 124(3), 127–137.
- [32] Shoimah, F., Usman, F., and Hariyani, S. (2021). Tsunami risk reduction in the new normal era based on community building in Watulimo, Indonesia. *IOP Conference Series: Earth and Environmental Science*, 916(1), 012033.
- [33] Shoimah, F., Usman, F., and Hariyani, S. (2022). Formulation of framework for evacuation of tsunami disaster after covid-19 pandemic on the south coast of Watulimo, Trenggalek. *TATALOKA*, 24(2), 131–140.
- [34] Teh, S. Y., Koh, H. L., and Lim, Y. H. (2019). High-resolution digital elevation and bathymetry model for tsunami run-up and inundation simulation in Penang. *Journal of Earthquake and Tsunami*, 13(05n06), 1941001.
- [35] Usman, F., Murakami, K., and Kurniawan, E. B. (2014). Study on reducing tsunami inundation energy by the modification of topography based on local wisdom. *Procedia Environmental Sciences*, 20, 642–650.
- [36] Usman, F., Eddi Basuki Kurniawan, M. Fathoni, and Rozikin, M. (2024). Tsunami disaster preparedness in tambakrejo village, sumber manjing wetan distric, Malang, Indonesia. *Evergreen*, 11(2), 1182–1189.
- [37] Fadly Usman, Keisuke Murakami, and Eddi Basuki Kurniawan. (2023). Disaster mitigation preparedness of Semeru volcano eruption. *International Journal of Advanced Technology and Engineering Exploration*, 10(108), 1524–1536.
- [38] Chen, G.-Y., Chiu, Y.-F., Lin, J.-H., Liu, C.-C., Chang, Y.-W., and Lien, C.-J. (2014). Combining tsunami hazard and vulnerability on the assessment of tsunami inundation probability in Taiwan. *Journal of Earthquake and Tsunami*, 8(3), 1440003.
- [39] Edgington, D. W. (2022). Planning for earthquakes and tsunamis: lessons from japan for British Columbia, Canada. *Progress in Planning*, 163, 100626.
- [40] Karima, S., Kongko, W., Khoirunnisa, H., Hendriyono, W., and Wibowo, M. (2021). Potential tsunami hazard on the coast of the Indonesia's new capital candidate. *IOP Conference Series: Earth and Environmental Science*, 832(1), 012044.

- [41] Kosaka, N., Koshimura, S., Terada, K., Murashima, Y., Kura, T., Koyama, A., and Matsubara, H. (2023). Decision-making support utilizing real-time tsunami inundation and damage forecast. *International Journal of Disaster Risk Reduction*, 94, 103807.
- [42] Wicaksono, A., D., and Usman, F. (2020). Investigation of tsunami impacted area from Anak Krakatoa Volcanic Eruption. *International Journal of GEOMATE*, 19(71), 235–241.